Materials Research. 2018; 21(2): e20170936
DOI: http://dx.doi.org/10.1590/1980-5373-MR-2017-0936

Annealing Effects on the Structural and Optical Properties of ZnO Nanostructures

Louise Patron Etcheverry[a], Wladimir Hernandez Flores[b], Douglas Langie da Silva[c], Eduardo Ceretta Moreira[b]*

[a]Programa de Pós-Graduação em Microeletrônica - PGMICRO, Universidade Federal do Rio Grande do Sul, Porto Alegre, RS, Brasil
[b]Universidade Federal do Pampa, Campus Bagé, Avenida Maria Anunciação Gomes de Godoy 1650, 96400-100, Bage, RS, Brasil
[c]Instituto de Física e Matemática, Universidade Federal de Pelotas, Pelotas, RS, Brasil

Received: October 16, 2017; Revised: December 13, 2017; Accepted: January 18, 2018

ZnO nanostructures were synthesized by a proteic sol-gel method, using zinc nitrate hexahydrate and gelatin as precursors. Size and shape evolution of ZnO nanostructures were achieved by annealing temperature in the range 250-1000 ºC. The crystalline structure, morphology and optical properties of the ZnO nanoparticles were characterized by X-Ray Diffraction (XRD), Raman Spectroscopy (RS), Fourier Transform Infrared Spectroscopy (FTIR), Scanning Electron Microscopy (SEM), Transmission Electron Microscopy (TEM), and room temperature Photoluminescence (PL). The result of structural characterization shows the formation of platelets and nanorods in the micro-scale and ZnO nanostructures with high quality hexagonal wurtzite crystal. Sharp peaks in RS after annealing temperature, related to wurtzite structure, were observed corroborating with XRD and TEM measurements. Room temperature PL spectra showed two contribution bands which peaked at ~380 nm, originating from the recombination of free excitons, and ~520 nm corresponding to the impurities and structural defects, like oxygen vacancies and zinc interstitial. The effects of annealing temperature in the structural and optical properties are detailed and the results compared among the experimental techniques. The high quality of the samples obtained by an alternative organic precursor method opens a low-cost route to technological applications of zinc oxide.

Keywords: *ZnO, structure, optical properties.*

1. Introduction

Zinc oxide (ZnO) is an important semiconductor material with a direct wide band gap (3.37 eV) and a large exciton binding energy at room temperature (about 60 meV)[1]. ZnO has attracted much attention due to its strong commercial importance, such as in solar energy conversion[2], photocatalysis[3], ultra-violet lasers[4], and gas sensors[5]. In this sense, ZnO has been postulated as a quasi-one-dimensional material with unique properties making it suitable for a series of applications. At this size range, it is expected that ZnO presents chemical and physical properties that are at variance from their bulk counterpart.

Nanostructured ZnO have been synthesized by distinct methods, such as ultrarapid sonochemical[6], hydrothermal synthesis[7], microwave assisted irradiate[8], sol-gel[9,10], and aqueous solution methods[11]. In all these cases, the materials properties are strongly dependent on the synthesis parameters. Some studies have demonstrated the role of gelatin as an organic matrix in controlling the nucleation/growth of ZnO nanoparticles[12-14] exploring changes in the gelatin concentration and gel formation after temperature reduction of the solution. In the present work, the results of structural/optical characterization are reported, using the synthesis of ZnO nanostructures via the proteic sol-gel method[15] that explores a Zn/Gelatin molar ratio in which Zn^{2+} does not exceed carboxyl and hydroxyl groups of gelatin. The proteic sol-gel method has advantages, such as short production time, low cost, and low synthesis temperature, leading to materials with high purity and homogeneity. The structural characterization of synthesized ZnO were performed by Scanning Electron Microscopy (SEM) and Transmission Electron Microscopy (TEM), Raman Spectroscopy, Fourier Transform Infrared Spectroscopy (FTIR), and X-Ray Diffraction (XRD). The optical characterization was done using a Photoluminescence (PL) technique. The experimental results point toward the synthesis of ZnO nanoparticles with high surface area and light emission in the range of 300 nm to 700 nm.

2. Experimental

2.1. Sample preparation

ZnO nanostructures were synthesized according to the method proposed by Meneses et al.[15] Gelatin solutions were prepared adding gelatin grains (1.25 g) to 20 ml of deionized

*e-mail: eduardomoreira@unipampa.edu.br

water (18.2 MΩ, Milli-Q, Millipore Corp.) under constant stirring at 45 ºC for 1 hour. After complete gelatin dilution, 0.5 g of zinc nitrate hexahydrate ($Zn(NO_3)_2.6H_2O$) was added to the solution and stirred for another 20 min. The gelatin resins were obtained from the resulting mixtures by solvent evaporation at 60 ºC, during 48 hours at atmospheric pressure in a preheated oven. The resulting product is highly brittle, as expected for gelatin in the solid state[16]. The gelatin resins were submitted to thermal decomposition for 3 hours at 250 ºC in air atmosphere. Finally, the thermal evolution of material was studied by annealing at temperatures ranging from 450 ºC to 1000 ºC for 3 hours.

2.2. Characterization

The morphology of the ZnO samples was characterized by SEM on a Shimadzu SSX-550 microscope. The TEM analyses were performed on a JEOL-2100 microscope operating at 200 kV in order to gain information about the shape and size of the ZnO nanostructures. The XRD measurements were performed on a RIGAKU ULTIMA IV diffractometer with Cu K_α radiation. The data was collected with a step size of 0.02º (2θ) in the range between 27º < 2θ < 80º with an integration time of 5 seconds. The FTIR spectra were recorded on a Shimadzu IR Prestige-21 in the transmission mode using powder samples made in the form of KBr pellets. The tablets were prepared using 100 mg of KBr and 1.8 mg of synthesized material. The acquisition was made at room temperature, with 45 scans and resolution of 4.0 cm^{-1}.

FT-Raman spectra were recorded on a Bruker MultiRam spectrometer using a liquid-nitrogen cooled Ge diode as detector. An air-cooled Nd:YAG-laser 1064 nm exciting line was applied as a light source. FT-Raman signal was collected in the back scattered direction, recorded over a range of 100 e 1700 cm^{-1}, using an operating spectral resolution of 1.5 cm^{-1}, and a laser power output of 100 mW.

Room temperature PL was performed by using Mini PL/Raman system, photon system USA, by means of a 5.0 eV (248.6 nm) laser excitation (about 50 mW and 20 μs pulse width), 1/8 m monochromator, and PMT detector resulting in a high resolution system (0.2 nm).

3. Results and Discussion

The effects of thermal degradation of gelatin resins at 250 ºC can be observed in the SEM image presented in the figure 1. The resulting material is highly brittle, formed by very dense agglomerates of platelet and flake-like structures, which is the typical morphology of resins after being burned in air.

The samples submitted to thermal degradation were annealed at temperatures between 450 ºC and 1000 ºC in order to study the thermal evolution of the material. Figure 2a presents an SEM of a sample annealed at 450 ºC. At the microscale, the material still presents a brittle-like character. However high magnification microscopy reveals that the material is formed by platelets and nanorods of ZnO (figure 2b). The nanorods present lengths of some microns with widths of nanometers. However these nanostructures change the morphology, and higher annealing temperatures (T = 700 ºC) lead to the formation of ZnO nanoparticles as present in the figure 2c. No traces of nanorods are observed pointing to the growth of nanoparticles at expense of nanorods. In order to obtain more detailed information about ZnO nanoparticles, TEM analysis were conducted on this sample. Figure 2d presents a bright field TEM image of ZnO nanoparticles. The shape of nanoparticles is dictated by their edges leading to squared or hexagonal-like nanoparticles. The nanoparticle size distribution (NSD) evaluated from a population of at least 300 nanoparticles are presented in the inset of figure 2d. Due to the shape fluctuation of ZnO nanoparticles, the NSD was obtained from the assumption of spherical nanoparticles. The monomodal NSD indicates that the nanoparticles present a mean diameter estimated to be 15 nm ± 1.1 nm. Annealing temperatures of 1000 ºC leads to the growth of the ZnO nanoparticle as depicted in the figures 2e and 2f. The nanoparticles still present fluctuations in shape, however the NSD under the assumption of spherical nanoparticles points to a mean diameter of 220 ± 60 nm. It is import to point out that after thermal decomposition of organic matter into collagen (at 250 ºC), no ZnO structures were observed. However, the nucleation of ZnO nanostructures in the matrix has already occurred at this temperature. The increase in temperature leads to a higher formation of nanoparticles as a result of a larger number of nuclei.

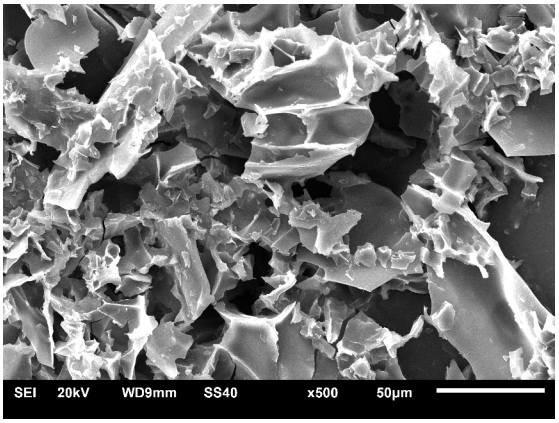

Figure 1. SEM image of a thermal decomposed sample at 250 ºC.

The XRD analysis of the samples annealed between 250 ºC and 1000 ºC are presented in the figure 3. The diffractogram for the sample thermally decomposed at 250 ºC indicating that the material at this stage is amorphous with the Zn atoms probably dispersed in the resulting material. On the contrary, the diffractogram from the ZnO sample annealed at 450 ºC presents Bragg reflections that can be indexed as polycrystalline hexagonal wurtzite structure

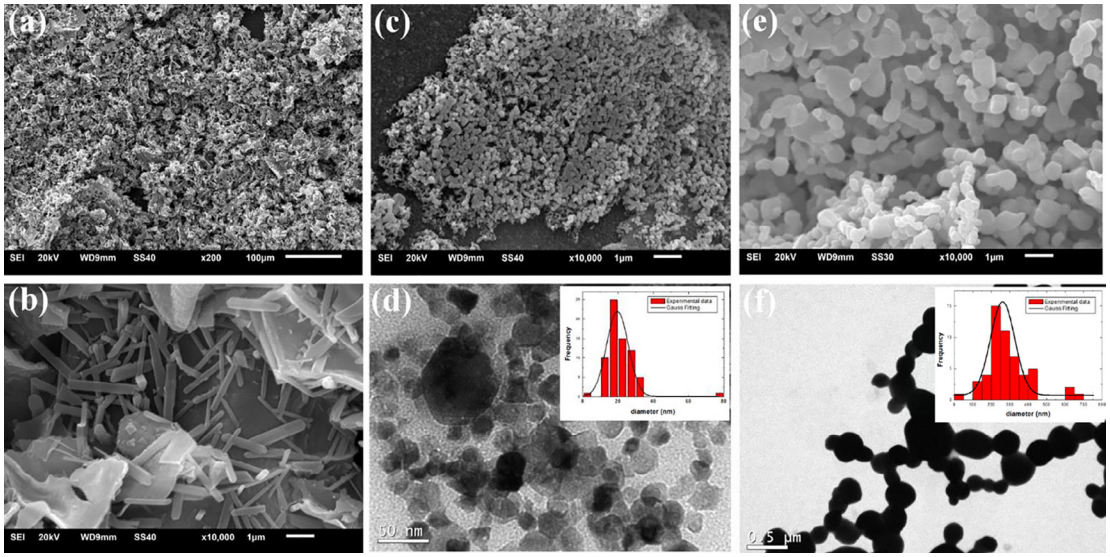

Figure 2. SEM images of the samples synthesized at temperatures of 450 ºC (a,b), 700 ºC (c), and 1000 ºC (e). TEM images of the samples at 700 ºC (d) and 1000ºC (f). Insets in (d,f): nanoparticle size distribution (NSD) evaluated from a population of at least 300 nanoparticles.

(JCPDS: 36-1451). The wurtzite structure has a hexagonal unit cell with lattice parameters a=b=3.25 Å and c=5.20 Å with space group C^4_{6v}. The structure is composed of two interpenetrating hexagonal close-packed (hcp) sublattices, each one consisting of one type of atom displaced with respect to each other along the threefold c-axis. The thermal evolution of samples at higher annealing temperatures is marked by a narrowing of the Bragg reflections from both grain growth and strain relief. Additionally, no significant changes to the position of the peaks in the diffractograms are observed, indicating that the basic unit atomic structure of the material is preserved under annealing at temperatures of interest in this work. Thus, the thermal evolution of ZnO samples is characterized by a morphological transformation, where ZnO nanorods and platelets turn into quasi spherical hexagonal wurtzite ZnO nanoparticles at higher annealing temperatures.

The effects of the XRD line broadening (size and shape of the crystallites and the presence of microstrain) are shown in figure 4, by means of Scherrer formula and a Williamson-Hall plot[17]. After instrumental correction of broadening, the expression of Scherrer to crystallite size (D) is

$$D = \frac{K\lambda}{\beta Cos\,\theta} \qquad (1)$$

where K is shape factor, λ is wavelength of the X-ray, β is the instrumental corrected integral breadth, and θ is the angle of reflection. In the case of the Williamson-Hall plot (WH-plot), the crystallite size (D) and strain (ε) broadening are deconvoluted by mathematical expression

$$\beta Cos\,\theta = \frac{K\lambda}{D} + 4\varepsilon Sen\,\theta \qquad (2)$$

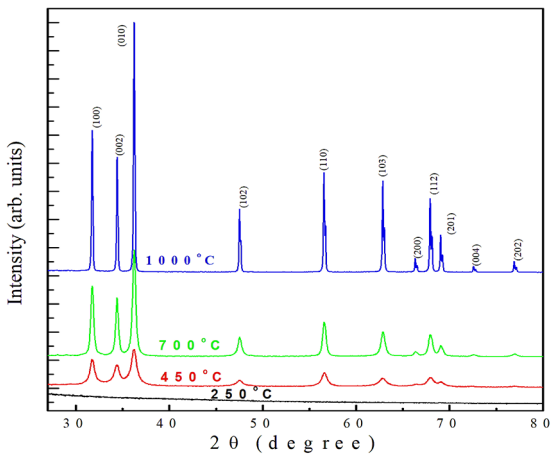

Figure 3. XRD patterns of the samples synthesized at temperatures of 250 ºC, 450 ºC, 700 ºC and 1000 ºC.

The narrowing of the Bragg reflections with the increase of the annealing temperature (observed in figure 3) can be observed in terms of the crystallite size (D) increase, as presented in figure 4a. Figure 4b shows the WH-plot of integral breadth ($\beta Cos\theta$) against $Sen\theta$ of samples annealed at 450 ºC, 700 ºC, and 1000 ºC, with a wide scatter of points and fit line (Eq. 2) with positive slope at lower temperatures. Qualitatively, this behavior indicates that the crystallites are anisotropic in shape and present domains with imperfections within the crystalline lattice (stacking faults, vacancies, dislocations, and others), respectively[18,19]. The analyses of WH-plot results are in good agreement with the TEM images, and point toward a smooth increase of the crystallite size of resulting nanostructures in the early range of annealing temperature (around 450 ºC), reaching values close to 20 nm at 700 ºC. Higher annealing temperatures

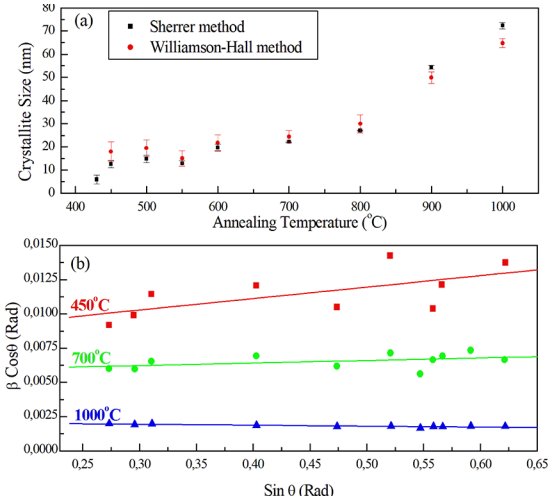

Figure 4. (a) crystallite size evolution as a function of annealing temperature by means of Scherrer formula and Williamson-Hall method; (b)Williamson-Hall plot of samples annealed at 450 ºC, 700 ºC and 1000 ºC.

lead to a significant increase of the crystallite, estimated to be around 70 nm for annealing at 1000 ºC. The apparent discrepancy between XRD and TEM analysis for the size of ZnO nanoparticles obtained at 1000 ºC is originated in the fundamentals of the techniques. It is well known that the XRD techniques present information about the size of crystallographic domain. On the other side, TEM analysis brings information about the size of nanoparticles in total. In this sense, larger size nanoparticles, as observed by TEM analysis, probably indicates that for this case the nanoparticles are not formed by only one crystallographic domain.

Figure 5 shows the FTIR spectra of ZnO samples annealed between temperatures ranging from 250 ºC to 1000 ºC. The spectra reveal a series of absorption peaks from 400 cm^{-1} to 2000 cm^{-1}. The FTIR spectrum for the sample annealed at 250 ºC presents absorption peaks at 1400 cm^{-1} and 1600 cm^{-1} from the asymmetric vibration of the CH_2 molecule and C=O stretching mode, respectively. The occurrence of these modes indicates the presence of organic residues from the synthesis and thermal degradation of the material at 250 ºC. Additionally, the absence of a peak in the region around 450 cm^{-1}, characteristic of the stretching mode of the Zn-O bond, indicates that no ZnO is formed at this temperature, which is in agreement with the XRD results. The FTIR spectra of samples annealed between 450 ºC and 1000 ºC presents distinct features when compared with the spectrum of the thermal decomposed sample. We can observe the presence of an absorption peak around 450 cm^{-1} pointing to the formation of the ZnO nanostructures and a small peak close to 1120 cm^{-1} relative to the incorporation of C-O groups to the ZnO surface during the measurements. The results clearly indicate that the ZnO nanostructures start to be formed at temperatures around 450 ºC. The increase in intensity of this peak with the annealing temperature is directly related with the increase in the number of Zn-O bonds.

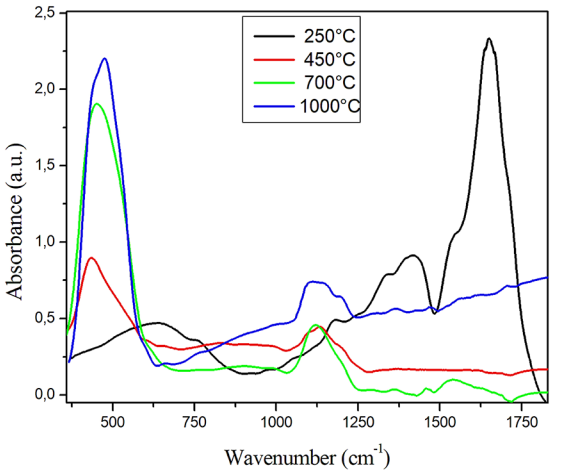

Figure 5. FTIR spectra of samples annealed in the range 250 ºC-1000 ºC.

In order to improve the vibrational properties, RS of thermally annealed ZnO samples were made. The Raman spectra of samples annealed at 500 ºC, 700 ºC, and 1000 ºC are shown in figure 6. In addition, table 1 shows the assignation and wavenumbers of pronounced modes, following results reported for bulk ZnO[20], of the first- and second-order Raman modes in the spectra of samples thermally annealed obtained by deconvolution of Lorentzian functions.

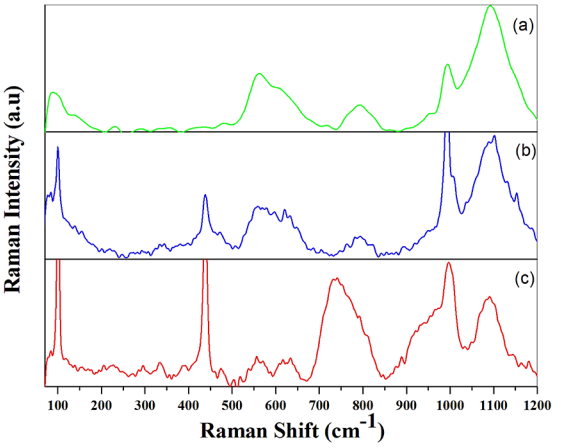

Figure 6. FT-Raman spectra of ZnO samples after thermal annealing at 500°C (a), 700°C (b) and 1000°C (c).

ZnO has a wurtzite structure, which belongs to the space group C^4_{6v} with two formula units per primitive cell where all atoms occupy C_{3v}. Zone center optical phonons predicted by group theory are $A_1+2E_2+E_1$, where A_1 and E_1 modes are polar and split into the transverse optical (TO) and longitudinal optical (LO) phonons. In addition, the E_2 mode consists of two modes: E_2^{high} which is associated with the vibration of oxygen atoms, and E_2^{low} which is associated with the Zn sublattice[21-23].

The effect of annealing temperature evolution shows that the major difference between the Raman spectra of

Table 1. Frequencies of first- and second-order FT-Raman spectra obtained at the samples annealed at 500 °C, 700 °C, and 1000 °C and compared with previous data in Ref.20, together with their assignments.

Frequency (cm^{-1})				
Ref. 20	500°C	700°C	1000°C	Process
99	92	99	100	E_2^{low}
203	_	203	205	2TA; $2E_2^{low}$
284	_	_	284	B_1^{high} - B_1^{low}
333	332	335	333	E_2^{high} - E_2^{low}
378	_	381	387	$A_1(TO)$
410	412	413	_	$E_1(TO)$
438	438	439	438	E_2^{high}
483	477	472	473	2LA
536	546	537	539	$2B_1^{low}$; 2LA
574	563	577	571	$A_1(LO)$
590	_	598	589	$E_1(LO)$
618	619	620	615	TA+TO
657	643	650	652	TA+TO
666	679	665	_	TA+TO
700	_	698	704	LA+TO
723	721	728	733	LA+TO
745	_	747	743	LA+TO
773	763	780	773	LA+TO
812	792	805	810	LA+TO
980	993	993	998	2TO
1044	1045	1041	1047	TO+LO
1072	1067	1078	1078	TO+LO
1105	1092	1101	1104	2LO
1158	1145	1154	1163	$2A_1(LO)$, $2AE_1(LO)$, $2LO$

samples annealed at 500 ºC and 700 ºC is the appearance of E_2^{high} mode at 438 cm^{-1}. This mode is characteristic of ZnO Raman spectra and is associated with the motion of oxygen and zinc sub-lattices in the wurtzite structure of the oxide[24], as the intensity of this mode increases the degree of crystallinity of ZnO oxide heightens. Similarly, with the increase of annealing until a temperature of 1000 ºC we observe a significant increase in the vibrational mode at 438 cm^{-1} in agreement with FTIR, which corroborates the good crystal quality of the samples as showed in the XRD analysis.

The vibration of the zinc sublatticeE_2^{low} is one of the most intense modes which peaked about 100 cm^{-1} and is the narrowest at 1000 ºC (5.2 cm^{-1}). The intensity of this vibrational mode heightens by increasing the annealing temperature. In addition, the position of the E_2 mode is sensitive to the stress along the structure of the oxide. The shift in the wavenumber towards larger values indicates the presence of compressive stress along the structure, while the shift of the wavenumber towards smaller values is representative of tensile stress. The invariance in the 438 cm^{-1} peak position by increasing the annealing temperature excludes the presence of these effects along the structure of the ZnO oxide over the whole range of studied temperatures.

In general, the structural characterization of the samples indicates that the thermal evolution of the ZnO oxide is marked by a morphological/structural transformation where the as-burned amorphous gelatin resins containing Zn atoms evolve to a system of quasi spherical crystalline ZnO nanoparticles after annealing at 1000 ºC.

In order to establish the optical properties of the ZnO nanoparticle, PL measurements were performed. Figure 7 shows the PL spectra of samples annealed at 450 ºC, 500 ºC, 700 ºC, and 1000 ºC. For annealing at temperatures lower than 450 ºC, PL spectra presents very broad light emissions due to the presence of the copolymer (not shown here). The copolymer contribution disappears when samples are annealed with temperatures higher than 450 ºC and ZnO bands emission at ultraviolet (UV) and visible (green/yellow) wavelengths compose the spectra. By annealing at 450 ºC a relatively weak and narrow UV emission band is observed around 380 nm (3.25 eV), called near-band-edge originating from the recombination of free excitons through

an exciton-exciton collision process. It is most pronounced at annealing in 450 ºC temperatures and decreases by increasing the annealing temperature. For an annealing temperature of about 500 ºC a spectrum transformation occurs, with the UV emission almost disappearing and emissions in the visible contribution band starting (about 400nm to 600nm) and peaked at 519 nm. This behavior is pronounced for annealing temperatures at 700 ºC and 1000 ºC. A small redshift (10 nm) is observed from 700 ºC to 1000 ºC, probably due to the increase of ZnO nanoparticles as well as a result of the morphology change transformations of the samples with increasing annealing temperature, as pointed out by TEM and XRD measurements.

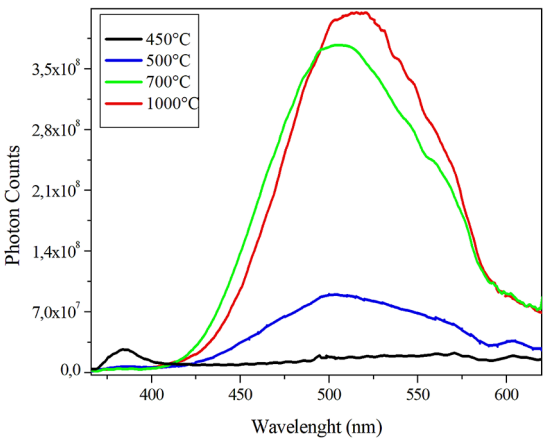

Figure 7. Effect of annealing temperature on the room temperature PL from ZnO nanoparticles annealed in air at 450 ºC, 500 ºC, 700 ºC and 1000 ºC. Excitation wavelength was 5eV.

The visible range emission is due to the impurities and structural defects, like oxygen vacancies and zinc interstitials in the ZnO crystals, and also known as deep level emission.

4. Conclusions

A systematic study on the structural and optical properties of ZnO nanostructures synthesized by proteic sol-gel method through thermal annealing ranging from 250 ºC to 1000 ºC was performed. ZnO nanoparticles start to be detected in samples annealed at 450 ºC as can be observed in the XRD, TEM, and FTIR. TEM analyses demonstrated that the thermal evolution of ZnO samples is characterized by a morphological transformation where ZnO nanorods and platelets turns into quasi spherical hexagonal wurtzite ZnO nanoparticles at a temperature of 1000 ºC. The vibrational mode (E_2^{high}) at 438 cm^{-1} at FT-Raman spectra corroborates the good crystal quality of the ZnO nanoparticles. The vibration mode E_2^{low} can be used as a probe to observe the effect of thermal evolution on the formation of ZnO nanoparticles. The annealed samples show light emission with a predominant band at about 520 nm due to defects in the ZnO crystals. The results of this study showed that the proteic sol-gel method is a very promising technique which presents a short production time, low cost, and low synthesis temperature, leading to materials with high purity and homogeneity. The systematic structural and optical analyses demonstrated the high potential of this technique on the ZnO nanoparticles and future technological applications.

5. Acknowledgments

The authors thank PROPESQ/UNIPAMPA and FAPERGS (PqG 12/2367-7) for financial support.

6. References

1. Sharma D, Rajput J, Kaitha BS, Kaur M, Sharma S. Synthesis of ZnO nanoparticles and study of their antibacterial and antifungal properties. *Thin Solid Films*. 2010;519(3):1224-1229.

2. Keis K, Magnusson E, Lindström H, Lindquist SE, Hagfeldt A. A 5% efficient photoelectrochemical solar cell based on nanostructures ZnO electrodes. *Solar Energy Materials and Solar Cells*. 2002;73(1):51-58.

3. Yang JL, An SJ, Park WI, Yi GC, Choi W. Photocatalysis using ZnO thin films and nanoneedles grown by metal-organic chemical vapor deposition. *Advanced Materials*. 2004;16(18):1661-1664.

4. Jin Y, Wang J, Sun B, Blakesley JC, Greenham NC. Solution-processed ultraviolet photodetectors based on colloidal ZnO nanoparticles. *Nano Letters*. 2008;8(6):1649-1653.

5. Xu J, Pan QY, Shun Y, Tian Z. Grain size control and gas sensing properties of ZnO gas sensor. *Sensors and Actuators B: Chemical*. 2000;66(3-1):277-279.

6. Shi Y, Zhu C, Wang L, Zhao C, Li W, Fung KK, et al. Ultrarapid Sonochemical Synthesis of ZnO Hierarchical Structures: From Fundamental Research to High Efficiencies up to 6.42% for Quasi-Solid Dye-Sensitized Solar Cells. *Chemistry of Materials*. 2013;25(6):1000-1012.

7. Liu B, Zeng HC. Hydrothermal synthesis of ZnO nanorods in the diameter regime of 50 nm. *Journal of the American Chemical Society*. 2003;125(15):4430-4431.

8. Al-Gaashani R, Radiman S, Tabet N, Daud AR. Effect of microwave power on the morphology and optical property of zinc oxide nano-structures prepared via a microwave-assisted aqueous solution method. *Materials Chemistry and Physics*. 2011;125(3):846-852.

9. Gómez-Núñez A, López C, Alonso-Gil S, Roura P, Vilà A. Study of a sol-gel precursor and its evolution towards ZnO. *Materials Chemistry and Physics*. 2015;162:645-651.

10. Heredia E, Bojorge C, Casanova J, Cánepa H, Craievich A, Kellermann G. Nanostructured ZnO thin films prepared by sol-gel spin-coating. *Applied Surface Science*. 2014;317:19-25.

11. Gomes MA, Valerio MEG, Rey JFQ, Macedo ZS. Comparative study of structural and optical properties of ZnO nanostructures prepared by three different aqueous solution methods. *Materials Chemistry and Physics*. 2013;142(1):325-332.

12. Zak AK, Majid WHA, Darroudi M, Yousefi R. Synthesis and characterization of ZnO nanoparticles prepared in gelatin media. *Materials Letters*. 2011;65(1):70-73.

13. Zhou J, Zhao F, Wang Y, Zhang Y, Yang L. Size-controlled synthesis of ZnO nanoparticles and their photoluminescence properties. *Journal of Luminescence*. 2007;122-123:195-197.

14. Kang SZ, Wu T, Li X, Mu J. A facile gelatin-assisted preparation and photocatalytic activity of zinc oxide nanosheets. *Colloids and Surfaces A: Physicochemical and Engineering Aspects*. 2010;369(3-1):268-271.

15. Meneses CT, Flores WH, Sasaki JM. Direct Observation of the Formation of Nanoparticles by in situ Time-Resolved X-ray Absorption Spectroscopy. *Chemistry of Materials*. 2007;19(5):1024-1027.

16. Kozlov PV, Burdygina GI. The structure and properties of solid gelatin and the principles of their modification. *Polymer*. 1983;24(6):651-666.

17. Mote VD, Purushotham Y, Dole BN. Williamson-Hall analysis in estimation of lattice strain in nanometer-sized ZnO particles. *Journal of Theoretical and Applied Physics*. 2012;6:6.

18. Majumdar A, Drache S, Wulff H, Mukhopadhyay AK, Bhattacharyya S, Helm CA, et al. Strain effects by surface oxidation of Cu_3N thin films deposited by DC magnetron sputtering. *Coatings*. 2017;7(5):64.

19. Scardi P, Leoni M, Delhez R. Line broadening analysis using integral breadth methods: a critical review. *Journal of Applied Crystallography*. 2004;37:381-390.

20. Cuscó R, Alarcón-Lladó E, Ibáñez J, Artús L, Jiménez J, Wang B, et al. Temperature dependence of Raman scattering in ZnO. *Physical Review B*. 2007;75:165202.

21. Šćepanović M, Grujić-Brojčin M, Vojisavljević K, Bernik S, Srećković T. Raman study of structural disorder in ZnO nanopowders. *Journal of Raman Spectroscopy*. 2009;41(9):914-921.

22. Ashkenov N, Mbenkum BN, Bundesmann C, Riede V, Lorenz M, Spemann D, et al. Infrared dielectric functions and phonon modes of high-quality ZnO films. *Journal of Applied Physics*. 2003;93(1):126-133.

23. Giri PK, Bhattacharyya S, Singh DK, Kesavamoorthy R, Panigrahi BK, Nair KGM. Correlation between microstructure and optical properties of ZnO nanoparticles synthesized by ball milling. *Journal of Applied Physics*. 2007;102(9):093515.

24. Arguello CA, Rousseau DL, Porto SPS. First-order Raman effect in wurzite-type crystals. *Physical Review Journals Archive*. 1969;181(3):1351-1363.